Dalton Transactions

Accepted Manuscript

ROYAL SOCIETY OF CHEMISTRY

www.rsc.org/dalton

Nickel L-edge and K-edge X-ray Absorption Spectroscopy of Non-Innocent $Ni[(S_2C_2(CF_3)_2]_2^n$ Series (n = -2, -1, 0): Direct Probe of Nickel Fractional Oxidation State Changes

Weiwei Gu[a,∇,+], Hongxin Wang[a,b,*,+], and Kun Wang[c,+]

[a] Physical Biosciences Division, Lawrence Berkeley National Laboratory, 1 Cyclotron Road, Berkeley, CA 94720

[b] Department of Chemistry, University of California, 1 Shields Avenue, Davis, CA 95616

[c] Corporate Strategic Research, ExxonMobil Research and Engineering Co., 1545 Rt. 22 East, Annandale, NJ 08801

A series of nickel dithiolene complexes $Ni[(S_2C_2(CF_3)_2]_2^n$ (n = -2, -1, 0) has been investigated using Ni L- and K-edge X-ray absorption spectroscopy (XAS). The L_3 centroid shifts about 0.3 eV for a change of one unit in the formal oxidation state (or 0.3 eV/oxi), corresponding to ~ 33% of the shift for Ni oxides or fluorides (about 0.9 eV/oxi). The K-edge XAS edge position shifts about 0.7 eV/oxi, corresponding to ~38% of that for Ni oxides (1.85 eV/oxi). In addition, Ni L sum rule analysis found the Ni(3d) ionicity in the frontier orbitals being 50.5%, 44.0% and 38.5% respectively (for n = -2, -1, 0), in comparison with their formal oxidation states (of Ni(II), Ni(III), and Ni(IV)). For the first time, direct and quantitative measurement of the Ni fractional oxidation state changes becomes possible for Ni dithiolene complexes, illustrating the power of L-edge XAS and L sum rule analysis in such a study. The Ni L-edge and K-edge XAS can be used in a complementary manner to better assess the oxidation states for Ni.

Key words:
Ni dithiolene complexes; X-ray absorption spectroscopy (XAS); Ni L-edge XAS; Sum rule analysis; Ni K-edge XAS.

∇ Current Address: UC Berkeley Extension, 1995 University Ave., Berkeley, CA 94704
+ All authors contributed equally

* Correspondence email: hxwang2@lbl.gov

Introduction

Metal dithiolene complexes have been a subject of extensive experimental and theoretical studies since the 1960s. [1-6] These complexes are relevant to bioinorganic chemistry,[4, 7, 8] and have potential applications in a wide range of areas from photo energy conversion,[9] to non-linear optics,[10, 11] to light–driven information devices.[12] The electronic structures of dithiolene complexes are unique. The 1,2-dithiolene ligand π orbitals interact with the metal *d* orbitals in the dithiolene complexes, giving frontier orbitals of mixed ligand and metal characters. The electrons are delocalized throughout the metal-ligand five-member rings. The dithiolene ligand can participate in the redox process of the complex and the metal often defies conventional oxidation state formalism in contrast to conventional coordination complexes; [4-6, 13-15] therefore the 1,2-dithiolene ligands are described as "non-innocent".

Oxidation state is one of the fundamental chemical properties, because the distribution of electron density in inorganic complexes determines their chemical and physical properties. Resolved oxidation states or electron / hole densities have helped understanding of many chemical processes, [4, 16, 17] while unresolved oxidation state has contributed to many longstanding controversies.[18-23] For Ni dithiolenes ($[Ni(S_2C_2R_2)_2]^{-2,-1,0}$, where R = H, CH_3, CN, Ph, CF_3 etc.), although Ni is formally Ni(II), Ni(III), and Ni(IV) when the dithiolene is viewed as ene-1,2-dithiolate, there is a large body of literature suggesting less than one unit oxidation state change for nickel should be expected as the complexes go through one-electron redox processes[1, 4, 15, 24, 25] due to the non-innocent nature of the ligand. Although the involvement of the dithiolene ligand in the redox processes is generally accepted, the extent of ligand contribution to the change of metal oxidation state varies depending on the nature of the complex. For example, for $[Cu(MNT)_2]^{-2,-1}$ (MNT = $S_2C_2(CN)_2$, 1,2-maleonitrile-1,2-dithiolate), the redox occurs mainly at Cu (instead of at ligand),[26] indicating that degree of ligand involvement in the redox process is sensitive to the metal center. Furthermore, the nature of the R group in the dithiolene ligand can also affect the extent of the ligand involvement in the redox process. Therefore experimental study for the individual dithiolene series is warranted in order to fully comprehend the change of metal oxidation state as the complex is reduced or oxidized.

X-ray absorption spectroscopy (XAS) monitors the electron transition from a core shell to a valence shell and is one of the best methods to investigate the element specific oxidation state. For studying electronic structures, such as the oxidation states, L-edge XAS ($2p \rightarrow 3d$) has several

advantages,[27, 28] which include: 1) direct observation of the 3*d* metal in the frontier orbitals[17, 29]; 2) quantitative measurement on 3*d* holes using the L sum rule analysis[17]; 3) rich and chemically informative spectra; and 4) dipole allowed transitions. Experimentally, higher energy resolution is easier to obtain from the synchrotron radiation source in the soft X-ray region. On the other hand, K-edge XAS is a bulk sensitive technique that can provide additional / complementary information on the oxidation states (via K-edge positions) as well as the metal-ligand distances (via Extended X-ray Absorption Fine Structures, EXAFS).

In this article, we report the first L-edge XAS study on a series of Ni dithiolene complexes: $(Ph_4As)_2Ni[S_2C_2(CF_3)_2]_2$ (**1**) [25], $(^nBu_4N)Ni[S_2C_2(CF_3)_2]_2$ (**2**) [25], and $Ni[S_2C_2(CF_3)_2]_2$ (**3**) [30]. For Ni dithiolenes, this also represents the first direct experimental and quantitative determination of Ni characters in the frontier orbital(s). Our experimental data are compared with published DFT calculations and other theoretically derived results from the Ni or S K-edge XAS. To confirm the L-edge measurements and to directly compare with the previous K-edge XAS data for other dithiolene systems, Ni K-edge XAS for **1**, **2** and **3** was also studied.

Results and discussions

Ni L-edge XAS overview

The L-edge XAS spectra for the complexes **1**, **2**, and **3** are shown in Fig. 1a (top panel). The general spectral features include: 1) two resonant absorption maxima at L_3 ($2p_{3/2}\rightarrow 3d$, ~853 eV) and L_2 ($2p_{1/2}\rightarrow 3d$, ~870 eV); and 2) a two-step non-resonant absorption between the pre-L_3 and post-L_2 regions (also called the edge jump). An expanded region with the non-resonant absorption background removed is illustrated in Fig. 1b (bottom panel). One of the important features for L-edge XAS is its chemically informative multiplet structures. Although the L-edge multiplets for **1**, **2**, and **3** are not as rich as those for ionic Ni oxides and fluorides [17] (because of their low-spin electronic configuration and their covalent nature), there are small but clear differences among **1**, **2** and **3** (Fig. 1b).

In general, similar to K-edge XAS, L_3 peak centroids shift to higher energy positions when the complexes are oxidized. This is attributed to the changes in core hole energy $\mathbf{H}_c$ and explained as a reduction in the 'valence electron screening'[28]. For example, Ni L_3 centroids for a series of Ni oxides and fluorides have been reported to shift up by ~0.9 eV per unit oxidation state change (or 0.9 eV/oxi for short in the following text).[17, 28] For the Ni dithiolene complexes

(Fig. 1b), the Ni L_3 absorption centroids are 853.3, 853.7 and 853.9 eV respectively for **1**, **2** and **3**. The average of 0.3 eV/oxi is approximately 33% of the shift for Ni oxides and fluorides (0.9 eV/oxi).[17] The Ni L_2 edge also shifts in the same direction. However, the exact shift in energy for the L_2 edge is difficult to quantify due to the nature of the transition (a shorter excited state lifetime and a broader peak width).[28]

The small peak at ~857eV is called the satellite feature (due to the ligand orbitals mixing with the Ni orbitals), which is often observed for covalent complexes.[28, 29] In an extreme case, metal carbonyl complexes can show a prominent peak due to the strong CO back-bonding to the metal *d* orbital[31, 32]. For reference, we present the Ni L-edge XAS for a Ni(I) carbonyl complex in Fig. 1c (light grey curve). Although the Ni-S satellite peaks for **1**, **2** and **3** are much less prominent than the one for Ni(I) carbonyl,[31, 32] these peaks are much more obvious in comparison with other Ni-S containing complexes.[28, 29] Being able to observe the clear albeit small peaks at ~857eV is consistent with the fact that these Ni dithiolene complexes having much more Ni-ligand mixing than typical Ni-S complexes.[1, 4, 15, 24, 25] It is also noticed that **2** and **3** have more complicated satellite features at ~857 eV than **1**, indicating more electron delocalization in **2** and **3** than in **1**. This observation is consistent with the fact that the complexes with higher oxidation states tend to have higher extent of metal-ligand mixing.

Integrated Ni L-edge XAS

Back to Fig. 1a, complex **1** formally has a $3d^8$ configuration and allows strong L_3 and L_2 absorption. As the formal oxidation state increases from Ni(II) **(1)** to Ni(III) **(2)** to Ni(IV) **(3)**, the L-edge intensity increases, although not as significant as that for Ni oxide or fluoride.[17] The normalized, integrated L absorption intensities for complexes **1, 2, 3** are 8.69, 11.33 and 13.25 respectively (see Table 2). While the multiplet analysis consists of information from both ground and final states, the sum rule value is a pure ground state property.[33, 34] There is a 'white light' sum rule [35] that states: the integrated intensity for an absorption edge is proportional to the total number of empty states (holes). According to this sum rule, the integrated Ni L absorption intensity should be proportional to the number of holes localized in the Ni(3*d*). This is one of the important advantages of L-edge XAS.[17]

To convert the L-edge intensities to the number of Ni(3*d*) holes, standard samples are needed. Two standards were used in this study: 1) Ni metal has an integrated L-edge intensity of

13.1[36] with a Ni(3*d*) hole of 1.5 (calculated from the band structure) [37, 38]; 2) NiO has an intensity of 14.7 [17, 39] with a calculated Ni(3*d*) hole of 1.72.[40, 41] Based on this calibration, one Ni(3*d*) hole corresponds to an integrated L intensity of ~8.6. Thus the measured numbers of Ni(3*d*) holes are 1.01, 1.32 and 1.54 for complexes **1**, **2**, **3** (Table 2). Fig. 2a shows a plot for the number of the "measured" Ni(3*d*) holes vs. the formal oxidation state. The parity line (shown in solid black line) is referred as the "100% ionicity" line. [17, 39] The positions for complexes **1**, **2**, and **3** are shown in Fig. 2a with the relative ionicity of 50.5%, 44.0%, and 38.5%, respectively (in comparison with the 100% ionicity line).

The increased charge localized on Ni(3*d*) is +0.31 (=1.32-1.01) going from **1** to **2**, and +0.22 (=1.54-1.32) from **2** to **3**, which is consistent with the Ni L-edge centroid shifts relative to ionic Ni complexes: 0.44 going from **1** to **2** (0.4/0.9 = 0.44); and 0.22 going from **2** to **3** (0.2/0.9 = 0.22).

The branching ratio, which is defined as $L_3/(L_2+L_3)$ (L_i signifies the integrated intensities for the L_i-edge peak), is another integrated spectral property. Previous experimental [42] and theoretical [43, 44] work pointed out that L_3 centroid is an indicator of oxidation states while the branching ratio reflects the electronic spin states for 3*d* metal complexes. Based on the measurements for various Ni complexes with different oxidation states and spin states, a correlation diagram has been established in previous publications, [39, 42] which are re-illustrated in Fig. 2b. With the circles as an eye guide, the data roughly illustrate the regions for the complexes with different electronic structures (oxidation states and spin states). The branching ratios for **1**, **2**, **3** are 0.70, 0.70 and 0.69 respectively – their locations in the correlation diagram (Fig. 2b) are all in the border region between the low spin and the high spin Ni(II) complexes, closer to low spin Ni(II) complexes. Although square-planar Ni complexes, especially Ni(II) complexes, tend to have a low spin electronic structure, the observation here indicates the high extent of Ni-ligand orbital mixing in complexes **1**, **2** and **3** could result in a more complex electronic structure.

Ni K-edge XAS overview

In addition to L-edge XAS, complexes **1**, **2**, and **3** were also evaluated with Ni K-edge XAS. The X-ray Absorption Near Edge Structure (XANES) spectra (3a) and their second derivatives (3b) are shown in Fig. 3, and the K absorption edge positions are listed in Table 1 (in comparison with L_3-edge XAS centroids). The K-edge positions shift to higher energy by 0.7

eV/oxi. This shift is similar to that for the Ni-MNT complexes[45] (*ca.* 1 eV/oxi going from $[Ni(MNT)_2]^{2-}$ to $[Ni(MNT)_2]^{1-}$), but much smaller than that for the Ni oxides (~1.85 eV/oxi; 3.7 eV going from Ni(II)O to KNi(IV)IO_6).[46] The shift obtained via K-edge XAS for **1**, **2** and **3** relative to that for the Ni oxide series (0.7/1.85=0.38) is similar to the ratio obtained with L-edge XAS above (0.3/0.9=0.33). This confirms our L-edge measurement reflects the samples' true properties, validating the L sum rule analysis.

The Ni-S distances obtained with EXAFS can also be used to infer the Ni oxidation state indirectly. For the compounds **1**, **2**, and **3**, the Ni-S coordination distances are 2.159 Å, 2.134 Å and 2.115 Å (see Table 3). These Ni-S distances fall within the range for typical 4-coordinated square-planar Ni complexes[47] (2.10 Å - 2.24 Å). The distance contracts about 0.022 Å/oxi, which is much smaller than the change for nickel oxides (*e.g.*, Ni-O distance changes 0.11 Å going from Ni(II) to Ni(III) and 0.08 Å from Ni(III) to Ni(IV)).[46] The trend is consistent with X-ray crystal structural data for $Ni[(S_2C_2(CF_3)_2]_2^n$ (the Ni-S distances decrease 0.011 Å/oxi from n=-1 to 0)[30] and with the EXAFS data for similar complexes,[48-51] such as $[Ni(S_2C_2Ph_2)_2]^{0,-1}$ and $[Ni(S_2C_2Me_2)_2]^{0,-1,-2}$ (*ca.* 0.02 Å /oxi). The smaller contraction of Ni–ligated atom distances in Ni dithiolenes (in comparison with that of nickel oxides) is consistent with the less drastic change of the oxidation state of Ni in the former as the complex is oxidized (*vide supra*).

L-edge XAS vs. K-edge XAS

In studying the electronic information, such as oxidation states, L-edge XAS has several distinct advantages as mentioned in the introduction. To illustrate this point, Fig. 3c shows the K-edge (c, upper curve) vs. L-edge (c, lower curve) XAS spectra for complex **1.** Both spectra are normalized to their non-resonant absorptions (edge jumps), and the L_3-edge XAS centroid is moved to align with the second inflection point of the K-edge XAS for easy comparison. Obviously, the L-edge XAS exhibits a much stronger resonant absorption and richer information than the K-edge XAS.

Several advantages of L-edge XAS are critical in studying extremely covalent complexes such as Ni dithiolenes. For example: 1) as the formal oxidation state is not an accurate metric to characterize different complexes, quantitative measurement on the oxidation state changes for Ni becomes critical as the complexes are reduced or oxidized; and L-edge XAS has such ability via the L sum rule analysis; 2) the Ni L-edge transition is primarily to the states with *d*-symmetry,

thus revealing electronic structures in the frontier orbital(s) directly. In comparison, the $1s \rightarrow 3d$ feature in K-edge XAS is a dipole-forbidden transition and often enhanced by *p-d* orbital mixing, making the quantitative measurements difficult, let alone the $1s \rightarrow 3d$ feature is almost invisible for a square-planar complex; 3) L-edge is more sensitive to peak position shift than K-edge because of the higher energy resolution in the soft X-ray source. In this study, the soft X-ray beam used for the Ni L-edge XAS (at Advanced Light Source BL4.0.2- ALS) has ~0.1 eV energy resolution, while the hard X-ray beam for the K-edge measurements (at Stanford Synchrotron Radiation Laboratory BL8.2 – SSRL) has ~1.0 eV energy resolution. Thus L-edge XAS measured energy shift for Ni dithiolenes (0.3 eV/oxi) is 3 times of its energy resolution (0.1 eV); while K-edge measured shift (0.7 eV/oxi) is only 70% of its energy resolution (1 eV). Thus L-edge XAS is critical in studying Ni dithiolenes because their spectral shifts are small.

On the other hand, Ni K-edge XAS is still useful because of its bulky sensitivity and its ability to study geometric structures (via EXAFS). It also probes different transitions, such as the $1s \rightarrow 4p_z$ peak (Fig. 3a and 3c) for a square-planar complex.[45, 52, 53]

Comparison with other dithiolene ligands

The non-innocent nature of dithiolene ligands stemmed from the fact that they often involve in the redox process of its coordination complexes. From our L-edge XAS results, Ni(3*d*) ionicity in the frontier orbitals are 50.5% (**1**), 44.0% (**2**), and 38.5% (**3**) respectively in comparison with their formal oxidation states, suggesting significant ligand involvement as the complexes go through the redox.

There are several important publications [1, 4, 5, 51] that quantified the Ni characters in the frontier orbitals for various Ni dithiolene complexes. Fig. 4 summarizes these calculated or derived percentages of Ni character in the frontier orbitals. Point (a)[1] represents earlier DFT results for $[Ni(S_2C_2H_2)_2]^{2-}$, which shows 9 electrons localized on Ni(3d), leading to one hole in its Ni(3*d*) orbital (or ~50% Ni(3d) ionicity in comparison with its formal oxidation states of +2). Series (b) represent the DFT calculations[51] for $Ni[S_2C_2(Me)_2]_2^n$ (n=-2, -1, 0), which showed a 13%, 19% and 39% character in the Ni d_{xz} orbital for the oxidation states of Ni(IV), Ni(III) and Ni(II). Series (c) [5] show results obtained from XAS and DFT for $[Ni(MNT)_2]^{-2,-1}$ by Solomon and co-workers. The ground state $[Ni(MNT)_2]^{-2}$ has 43% character in Ni $3d_{x2-y2}$, 44% in S $3p_\sigma$, and the rest (13%) over other atoms in the NMT ligand.[5] For $[Ni(MNT)_2]^{-1}$, LUMO (lowest

unoccupied molecular orbital) has 40% in Ni, 46% in S, 14% in other atoms; [5] the half-filled HOMO (highest occupied molecular orbital) has 31% in Ni, 51% in S and 18% in other atoms.[5] In 2003, Solomon and coworkers re-evaluated the series in (b)[4] from the ligand (S) point of view (with S pre-K-edge XAS measurements and DFT calculations). The ground-state wave functions of the Ni(II) complex has 77% S character in its LUMO. The formally Ni(III) complex has 59% or 71% S character depending on its frontier orbitals. Similarly, the formally Ni(IV) complex has 57% or 67% S character. All the three complexes show a strong ligand (S) character in their frontier orbitals.

The above discussions revealed that the Ni characters in the frontier orbitals are all ≤50%. However, each series of Ni dithiolene complexes [1, 4, 5, 13, 14, 23, 51] has very different Ni characters in the frontier orbitals. In addition, within each study, differences also exist between results derived from XAS measurements and those from DFT calculations. Therefore direct and quantitative measurement on each series of dithiolene ligands (with different R groups) is necessary for obtaining a complete picture to understand the oxidation state change for Ni during the redox process for Ni dithiolene complexes. Our L-edge XAS measurement on $Ni[S_2C_2(CF_3)_2]_2^{-2,-1,0}$ is the first such experimental determination of Ni(3*d*) holes in the metal-ligand orbitals. This work also provides an example of applying Ni L-edge XAS on extremely low iconicity (≤50%) Ni-S coordination systems. With the advancement of liquid cell technology for soft X-ray experiments,[54] *in-situ* / *operando* and quantitative characterization of the Ni electronic structure for $[Ni(S_2C_2R_2)_2]^{Z-}$ in solution may be possible in the near future.

Summary

L-edge and K-edge XAS are used to study the electronic structure of a series of Ni dithiolene compounds $Ni[(S_2C_2(CF_3)_2]_2^n$ (n = -2, -1, 0). For a change of one unit in the formal oxidation state, the L_3 centroid shifts 0.3 eV, which is ~ 33% of that for Ni oxides or fluorides (0.9 eV/oxi). The L sum rule analysis further revealed 38-50% Ni ionicities for these Ni dithiolenes. The L_3 centroid - branching ratio correlation diagram indicates that Ni in all these complexes are close to a low spin Ni(II) species. The K-edge XAS edge position shifts about 0.7 eV/oxi., corresponding to 38% of that for Ni oxides (1.85 eV/oxi). K-edge EXAFS showed ~ 0.022 Å Ni-S bond shortening as the compound is oxidized by one electron (0.022 Å/oxi), which is much smaller than that for Ni-O distances in Ni oxides (~ 0.11 Å/oxi).

Our L-edge and K-edge XAS studies gave consistent results in assessing the oxidation state changes for Ni in these Ni dithiolenes. For the first time, L-edge XAS and L sum rule analysis make it possible to determine the fractional oxidation state changes directly and quantitatively for the above Ni dithiolenes. This work is also the first L-edge XAS study and the first L-edge vs. K-edge comparison on a series of extremely covalent Ni dithiolene complexes. We also showed that L-edge and K-edge XAS can be used in a complementary manner to better assess the fractional oxidation state changes of Ni in the dithiolene complexes.

Acknowledgements

The research is supported by the National Institutes of Health (GM-65440, to Prof. Stephen P. Cramer at University of California at Davis). We thank Prof. Cramer for the overall support for this work, Prof. C. G. Riordon in University of Delaware for providing the reference sample $[PhTt^{tBu}]Ni^{(I)}CO$. ALS and SSRL are supported by the Department of Energy, Office of Basic Energy Sciences. This research is also part of the advanced biological experimental X-ray spectroscopy program (ABEX), which is supported by the U.S. Department of Energy, Office of Biological and Environmental Research. All the LBNL work is under the DOE/LBNL contract DE-AC02-05CH11231.

Experimental

Samples

The nickel dithiolene complexes used in this study, $(Ph_4As)_2Ni[S_2C_2(CF_3)_2]_2$(**1**) [25], $(^nBu_4N)Ni[S_2C_2(CF_3)_2]_2$ (**2**) [25] and $Ni[S_2C_2(CF_3)_2]_2$ (**3**) [30] were synthesized following literature methods. The solid samples were sealed under nitrogen inside ampules and the seals opened inside a nitrogen atmosphere glovebox prior to XAS measurements. The sample powder was prepared inside the glovebox although K-edge XAS measurement was done under ambient conditions. The reference Ni(I) carbonyl sample[55] ($[PhTt^{tBu}]Ni^{(I)}CO$) was synthesized in Riordon's Lab at University of Delaware. Energy calibration samples NiF_2 and Ni foil were purchased from Sigma-Aldrich and used as received (purity = 99.5%).

L-edge XAS measurements

Ni L-edge spectra were measured at the beamline 4.0.2[56] at ALS. The measurement chamber was maintained at a vacuum of $2x10^{-9}$ torr, enabling windowless operation between the storage ring, the sample and the detector[29]. The entrance and exit slits were set at 10 μm which corresponds ΔE=0.1 eV. In soft X-ray region, the proper thickness for transmission measurement is only a few thousand Å, and the homogenous samples are difficult to prepare. Therefore the spectra were recorded in total electron yield mode [57]. While the monochromator was scanned across the intended energy region, the total electron yield signal from the sample (I_E) was measured using a Galileo 4716 channeltron electron multiplier. The incident beam intensity (I_0) was measured via a gold plated grid in the entrance of the incident beam. The (I_E/I_0) was used as the intensity in each raw scan. To avoid possible radiation damage, a defocused beam of 1x1 mm^2 was used and the spot was moved for every scan. Under these conditions, there is no spectral change from scan to scan.

The XAS scans were recorded with a step size of 0.1 eV and an integration time of 3 sec/pt. The spectral reproducibility was within 0.1 eV. Each final spectrum was the average of 4 (I_E/I_0) scans. The Ni L-edge XAS was calibrated using the L_3 peak of NiF_2 at 852.7 eV. [17]

The Ni L-edge data processing[17] involves subtraction of a no-structure background absorption for blank sample holder (carbon tape) and tilt of the remaining linear baseline. Such spectrum was then normalized to their invariant edge jumps between the pre-L_3 and the post-L_2 regions to yield the spectra in Fig. 1a.

The two-step non-resonance baselines were then removed to obtain resonant absorption spectra (see Fig. 1b), from which the spectral multiplets were analyzed and the absorption intensities were integrated over the regions of L_3 (851-858 eV) and L_2 (868-874 eV) edges.

Correlation diagram (Fig. 2b) is another integrated L-edge properties, which relates the L_3 centroids to the Ni oxidation states and the branching ratio of $L_3/(L_2+L_3)$ to the Ni spin states statistically. The L_3 and L_2 represent the integrated intensities at edges L_3 and L_2 respectively.

K-edge XAS measurements

Ni K-edge XAS data for Ni dithiolenes were collected on at the beamline 2-3 at SSRL. Si(111) monochromator crystals were used with 2 mm beam slits for EXAFS scans and 1mm slits for XANES spectra. The energy calibration was performed *in-situ* using a Ni foil and using

a typical 3 ion chamber setup [58] - with the Ni dithiolene sample between I_0 and I_1 and Ni foil between I_1 and I_2. The energy was calibrated by setting the first inflection point of the Ni foil spectrum to 8331.6 eV. High order harmonic beam was rejected by detuning the second monochromator crystal to a position where the beam flux becomes 50% of its maximum value. XANES XAS and EXAFS data were collected at transmission mode and each spectrum was the sum of three 20-min scan.

K-edge EXAFS measurement and analysis are performed following the published standard procedure[58, 59] (analysis software=EXAFSPAK[59] and k = 1 - 14.5 Å).

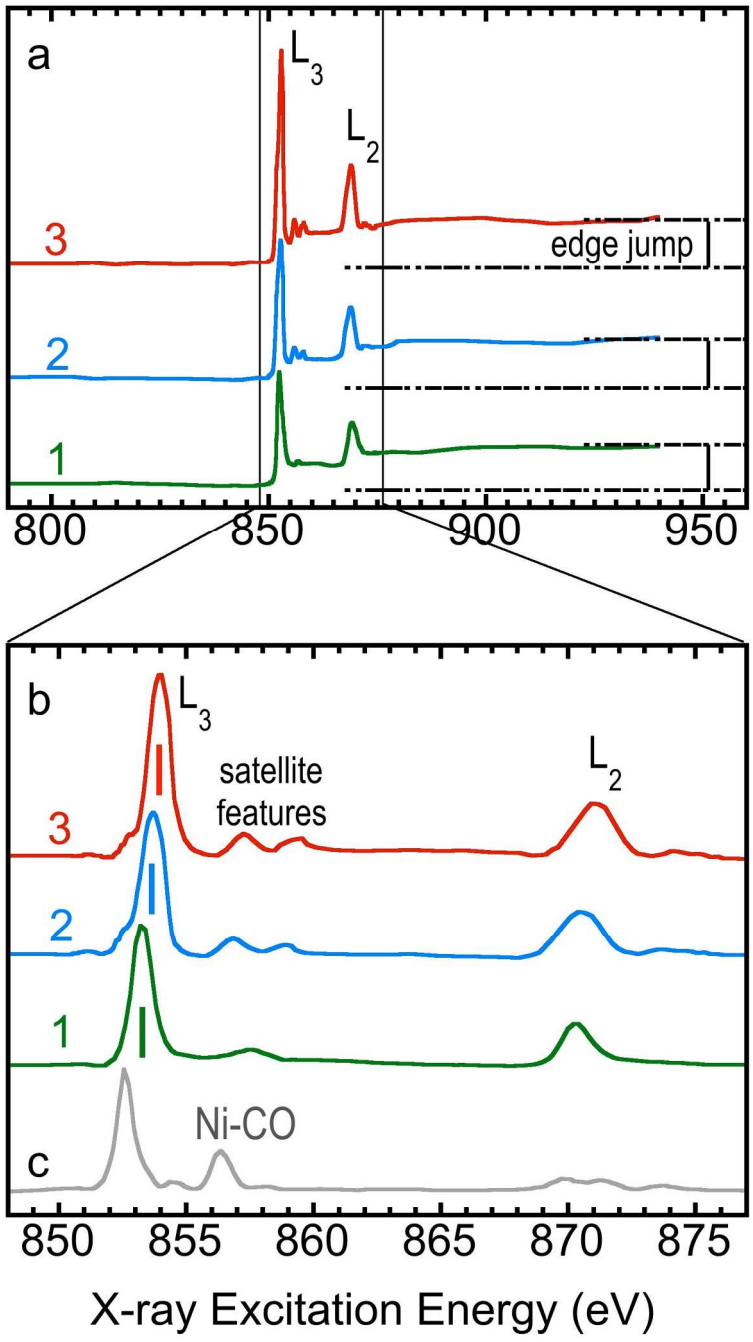

Fig. 1.

The wide energy range (a), and the expanded and non-resonant edge jump removed (b) Ni L-edge XAS spectra for complexes **1** (green) **2** (blue), and **3** (red). The L-edge XAS for a reference Ni(I) carbonyl compound (light grey) is shown for comparison (c).

.

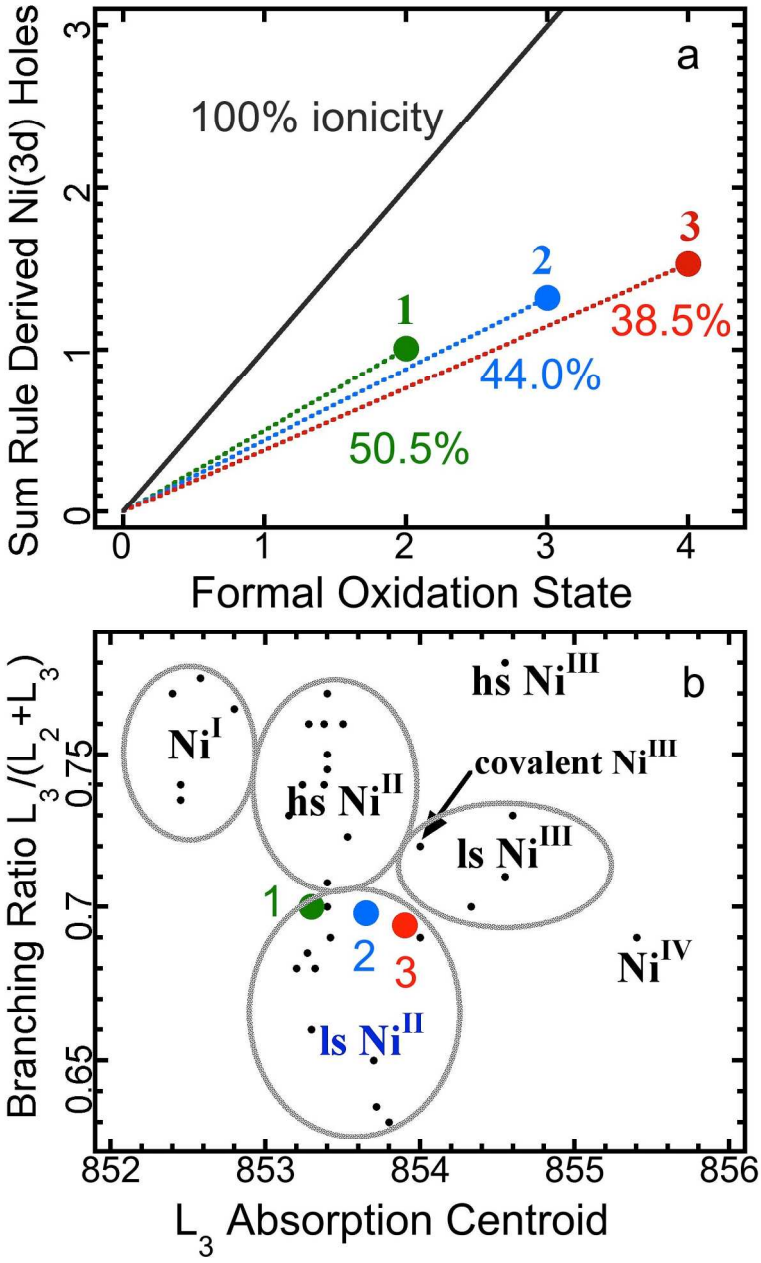

Fig. 2.

(a) Ni L sum rule analyzed numbers of Ni(3d) holes vs. formal oxidation states for **1** (green), **2** (blue), and **3** (red). The black line indicates the 100% iconicity; and (b) the correlation diagram of L_3 absorption centroids vs. branching ratios of $[L_3/(L_2+L_3)]$, and the positions for complexes **1**, **2** and **3.**

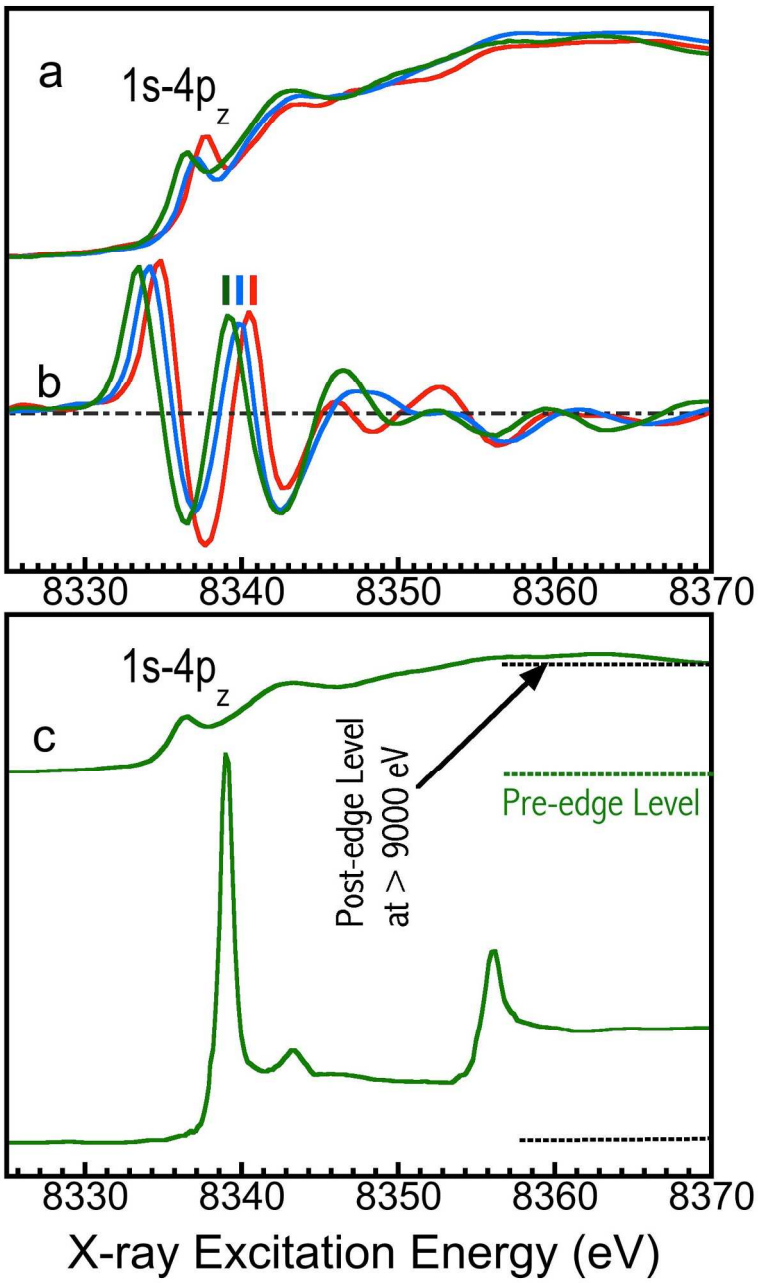

Fig. 3

The K-edge XAS spectra for **1** (green), **2** (blue), **3** (red) (a); their second derivatives (b); and the comparison of K-edge (c, upper curve) vs. L-edge (c, lower curve) XANES spectra for complex **1**. For (c), each spectrum is normalized to its edge jump, and the L-edge XAS is moved to align with the second inflection point of the K-edge XAS at 8339.1 eV.

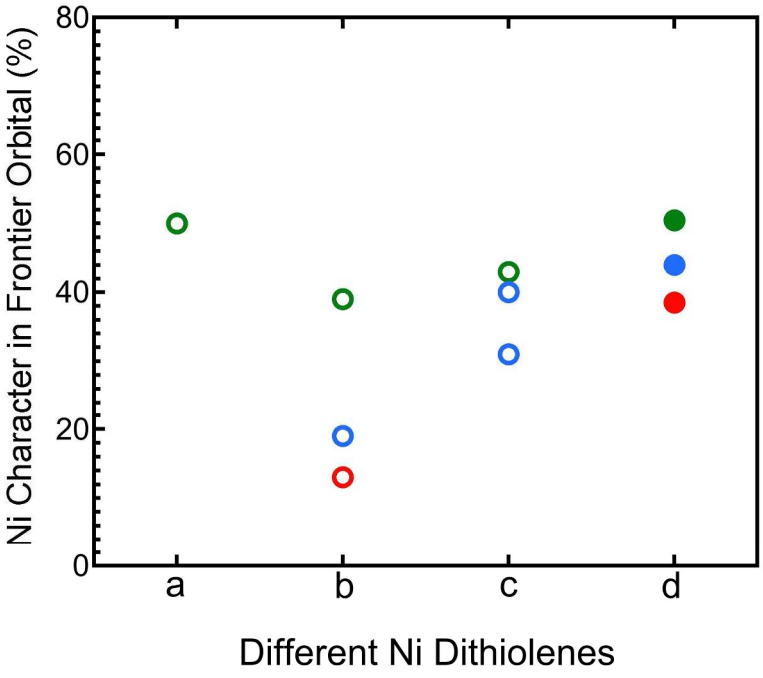

Fig. 4

Ni character percentage in the frontier orbitals in various Ni dithiolene complexes: (a)[1] $Ni[(S_2C_2H_2]^{2-}$; (b)[51] $[NiS_2C_2(Me)_2]^{0,-1,-2}$; (c)[5] $[Ni(MNT)_2]^{0,-1,-2}$; and (d) the direct quantitative measurements from this work (solid symbols). The colors are used to indicate the formal oxidation states of Ni(II) (green), Ni(III) (blue) and Ni(IV) (red) respectively.

Table 1. K-edge and L-edge positions of complexes **1**, **2**, and **3** vs. the ionic Ni oxide complexes

	complex **1** edge position	complex **2** edge position	complex **3** edge position	ΔE_A (per unit redox for **1**, **2** and **3**)	ΔE_B (per unit redox for Ni oxide)	$\Delta E_A/\Delta E_B$ %
Ni L-edge	853.3	853.7	853.9	+0.30	+0.90	33%
Ni K-edge	8339.1	8339.8	8340.5	+0.70	+1.85	38%

Table 2. Integrated L-edge intensities and L sum rule analyzed Ni(3d) holes for **1**, **2**, and **3**.

Compounds	Integrated Intensity	Ni(3d) Holes	Ni(3d) Ionicity
1	8.69 ± 0.99	1.01 ± 0.12	50.5 %
2	11.33 ± 1.70	1.32 ± 0.20	44.0 %
3	13.25 ± 1.95	1.54 ± 0.23	38.5 %

Table 3. The EXAFS measured Ni-S distances for Ni dithiolene complexes **1**, **2**, and **3**.

Compounds	Ligands	R(Å)	σ^2 (10^{-1}Å^2)
1	4S	2.159	2.70
2	4S	2.134	2.24
3	4S	2.115	2.22

References

1. C. Lauterbach and J. Fabian, *European Journal of Inorganic Chemistry*, 1999, 1995-2004.
2. J. A. McCleverty, *Progr. Inorg. Chem.*, 1968, **10**, 49-221.
3. G. N. Schrauzer, *Accounts Chem. Res.*, 1969, **2**, 72-80.
4. R. K. Szilagyi, B. S. Lim, T. Glaser, R. H. Holm, B. Hedman, K. O. Hodgson and E. I. Solomon, *Journal of the American Chemical Society*, 2003, **125**, 9158-9169.
5. R. Sarangi, S. D. George, D. J. Rudd, R. K. Szilagyi, X. Ribas, C. Rovira, M. Almeida, K. O. Hodgson, B. Hedman and E. I. Solomon, *Journal of the American Chemical Society*, 2007, **129**, 2316-2326.
6. K. Ray, S. D. George, E. I. Solomon, K. Wieghardt and F. Neese, *Chemistry-a European Journal*, 2007, **13**, 2783-2797.
7. J. Reedijk and E. Bouwman, *Bioinorganic catalysis*, Marcel Dekker, Inc., New York :, 1999.
8. J. Yadav, S. K. Das and S. Sarkar, *Journal of the American Chemical Society*, 1997, **119**, 4315-4316.
9. W. Paw, S. D. Cummings, M. A. Mansour, W. B. Connick, D. K. Geiger and R. Eisenberg, *Coordination Chemistry Reviews*, 1998, **171**, 125-150.
10. C. T. Chen, S. Y. Liao, K. J. Lin and L. L. Lai, *Advanced Materials*, 1998, **10**, 334-338.
11. C. S. Winter, S. N. Oliver, J. D. Rush, C. A. S. Hill and A. E. Underhill, *Journal of Applied Physics*, 1992, **71**, 512-514.
12. U. T. Muellerwesterhoff, B. Vance and D. I. Yoon, *Tetrahedron*, 1991, **47**, 909-932.
13. H. B. Gray, *Transition Metal Chem.*, 1965, **1**, 239-287.
14. E. I. Solomon, B. Hedman, K. O. Hodgson, A. Dey and R. K. Szilagyi, *Coordination Chemistry Reviews*, 2005, **249**, 97-129.
15. D. C. Olson, V. Mayweg and G. N. Schrauzer, *J. Am. Chem. Soc.*, 1966, **88**, 4876-4882.
16. S. J. George, M. D. Lowery, E. I. Solomon and S. P. Cramer, *Journal of the American Chemical Society*, 1993, **115**, 2968-2969.
17. H. X. Wang, P. H. Ge, C. G. Riordan, S. Brooker, C. G. Woomer, T. Collins, C. A. Melendres, O. Graudejus, N. Bartlett and S. P. Cramer, *Journal of Physical Chemistry B*, 1998, **102**, 8343-8346.
18. S. J. Lippard and J. M. Berg, *Principles of Bioinorganic Chemistry*, University Science Books, Mill Valley, CA, 1994.
19. I. Bertini, Gray, J. H. B., L. S. and J. S. Valentine, *Bioinorganic Chemistry*, University Science Books, Mill Valley, CA, 1994.
20. S. P. J. Albracht, *Biochimica Et Biophysica Acta-Bioenergetics*, 1994, **1188**, 167-204.
21. R. Cammack, V. M. Fernandez and E. C. Hatchikian, in *Inorganic Microbial Sulfur Metabolism*, eds. J. LeGall and H. D. Peck, Jr., Academic Press Inc., San Diego, CA, Editon edn., 1994, vol. 243, pp. 43-67.
22. I. J. Pickering, G. N. George, J. T. Lewandowski and A. J. Jacobson, *Journal of the American Chemical Society*, 1993, **115**, 4137-4144.
23. C. L. Coyle and E. I. Stiefel, in *The Bioinorganic Chemistry of Nickel*, ed. J. R. Lancaster Jr., VCH Publishers, New York, Editon edn., 1988, pp. 1-28.
24. E. Billig, R. Williams, I. Bernal, J. H. Waters and H. B. Gray, *Inorg. Chem.*, 1964, **3**, 663-666.
25. A. Davison and R. H. Holm, *Inorg. Synth.*, 1967, **10**, 8-26.

26. R. Sarang, S. D. George, D. J. Rudd, R. K. Szilagy, X. Ribas, C. Rovira, M. Almeida, K. O. Hodgson, B. Hedman and E. I. Solomon, *J. Am. Chem. Soc.*, 2007, **129**, 2316-2326.
27. S. P. Cramer, F. M. F. Degroot, Y. Ma, C. T. Chen, F. Sette, C. A. Kipke, D. M. Eichhorn, M. K. Chan, W. H. Armstrong, E. Libby, G. Christou, S. Brooker, V. Mckee, O. C. Mullins and J. C. Fuggle, *Journal of the American Chemical Society*, 1991, **113**, 7937-7940.
28. S. P. Cramer, H. X. Wang, C. Bryant, M. Legros, C. Horne, D. Patel, C. Ralston and X. Wang, in *Spectroscopic Methods in Bioinorganic Chemistry*, eds. E. I. Solomon and K. O. Hodgson, American Chemical Society, Washington, D. C., Editon edn., 1998, vol. 692, pp. 154-178.
29. H. X. Wang, C. Y. Ralston, D. S. Patil, R. M. Jones, W. Gu, M. Verhagen, M. Adams, P. Ge, C. Riordan, C. A. Marganian, P. Mascharak, J. Kovacs, C. G. Miller, T. J. Collins, S. Brooker, P. D. Croucher, K. Wang, E. I. Stiefel and S. P. Cramer, *Journal of American Chemical Society*, 2000, **122**, 10544-10552.
30. K. Wang, A. O. Patil, S. Zushma and J. M. McConnachie, *J. Inorg. Biochem.*, 2007, **101**, 1883.
31. H. Liu, Guo, Y. Yin, A. Augustsson, C. Dong, J. Nordgren, C. Chang, P. Alivisatos, G. Thornton, D. F. Ogletree, F. G. Requejo, F. de Groot and M. Salmeron, *Nano Letters*, 2007, **7**, 1919-1922.
32. H. Wang, S. M. Butorin, A. T. Young and J. Guo, *The Journal of Physical Chemistry C*, 2013, **117**, 24767-24772.
33. C. Bonnelle, *Compt. rend.*, 1959, **248**, 2324-2326.
34. Y. Cauchois and C. Bonnelle, *Compt. rend.*, 1957, **245**, 1230-1234.
35. A. F. Starace, *Phys. Rev. B*, 1972, **[3]5**, 1773-1784.
36. J. Stohr and R. Nakajima, *IBM J. Res. Dev.*, 1998, **42**, 73-88.
37. O. Eriksson, B. Johansson, R. C. Albers, A. M. Boring and M. S. S. Brooks, *Phys. Rev. B: Condens. Matter*, 1990, **42**, 2707-2710.
38. P. Soederlind, O. Eriksson, B. Johansson, R. C. Albers and A. M. Boring, *Phys. Rev. B: Condens. Matter*, 1992, **45**, 12911-12916.
39. H. X. Wang, D. S. Patil, W. W. Gu, L. Jacquamet, S. Friedrich, T. Funk and S. P. Cramer, *Journal of Electron Spectroscopy and Related Phenomena*, 2001, **114**, 855-863.
40. P. S. Bagus, R. Broer, C. de Graaf and W. C. Nieuwpoort, *Journal of Electron Spectroscopy and Related Phenomena*, 1999, **99**, 303-319.
41. J. Choisnet, R. A. Evarestov, Tupitsyn, II and V. A. Veryazov, *Journal of Physics and Chemistry of Solids*, 1996, **57**, 1839-1850.
42. C. Y. Ralston, H. X. Wang, S. W. Ragsdale, M. Kumar, N. J. Spangler, P. W. Ludden, W. Gu, R. M. Jones, D. S. Patil and S. P. Cramer, *Journal of the American Chemical Society*, 2000, **122**, 10553-10560.
43. F. M. F. Degroot, J. C. Fuggle, B. T. Thole and G. A. Sawatzky, *Physical Review B-Condensed Matter*, 1990, **42**, 5459-5468.
44. F. deGroot and G. vanderLaan, *Journal of Electron Spectroscopy and Related Phenomena*, 1997, **86**, 25-40.
45. M. K. Eidsness, R. J. Sullivan and R. J. Scott, in *The Bioinorganic Chemistry of Nickel*, ed. J. R. Lancaster Jr., VCH Publishers, New York, Editon edn., 1988, pp. 73-91.
46. A. N. Mansour and C. A. Melendres, *Journal of Physical Chemistry A*, 1998, **102**, 65-81.

47. M. R. Churchill, J. Cooke, J. P. Fennessey and J. Wormald, *Inorganic Chemistry*, 1971, **10**, 1031-1035.
48. C. Mahadevan, M. Seshasayee, P. Kuppusamy and P. T. Manoharan, *J. Crystallogr. Spectrosc. Res.*, 1984, **14**, 179-191.
49. M. Megnamisibelombe and B. Nuber, *Bulletin of the Chemical Society of Japan*, 1989, **62**, 4092-4094.
50. D. Sartain and M. R. Truter, *J. Chem. Soc. A*, 1967, 1264-1272.
51. B. S. Lim, D. V. Fomitchev and R. H. Holm, *Inorganic Chemistry*, 2001, **40**, 4257-4262.
52. C. Bagyinka, J. P. Whitehead and M. J. Maroney, *Journal of the American Chemical Society*, 1993, **115**, 3576-3585.
53. Z. J. Gu, J. Dong, C. B. Allan, S. B. Choudhury, R. Franco, J. J. G. Moura, J. Legall, A. E. Przybyla, W. Roseboom, S. P. J. Albracht, M. J. Axley, R. A. Scott and M. J. Maroney, *Journal of the American Chemical Society*, 1996, **118**, 11155-11165.
54. J. Guo, T. Tong, L. Svec, J. Go, C. Dong and J.-W. Chiou, *J. Vac. Sci. Technol. A*, 2007, **25**, 1231-1233.
55. P. H. Ge, C. G. Riordan, G. P. A. Yap and A. L. Rheingold, *Inorganic Chemistry*, 1996, **35**, 5408-5409.
56. A. T. Young, E. Hoyer, S. Marks, V. Martynov, H. A. Padmore, D. Plate and R. Schlueter, *Review of Scientific Instruments*, 1996, **67**.
57. J. Stohr, *NEXAFS Spectroscopy*, Springer-Verlag, New York, NY, 1992.
58. J. E. Penner-Hahn, *Coordination Chemistry Reviews*, 1999, **192**, 1101-1123.
59. G. G. George, *EXAFSPAK*, http://xafs.org/Software/EXAFSPAK, 2013.